Biochimica et Biophysica Acta 1838 (2014) 1730–1737

Contents lists available at ScienceDirect

Biochimica et Biophysica Acta

journal homepage: www.elsevier.com/locate/bbamem

Rapid evaluation of a protein-based voltage probe using a field-induced membrane potential change

Hidekazu Tsutsui [a,b,*], Yuka Jinno [a], Akiko Tomita [a], Yasushi Okamura [a]

[a] Laboratory of Integrative Physiology, Graduate School of Medicine, Osaka University, Suita, Osaka 565-0871, Japan
[b] Formation of and information processing by neural networks, and control, PRESTO, Japan Science and Technology Agency (JST), 4-1-8 Hon-cho, Kawaguchi, Saitama 351-0198, Japan

ARTICLE INFO

Article history:
Received 20 December 2013
Received in revised form 27 February 2014
Accepted 10 March 2014
Available online 16 March 2014

Keywords:
Genetically-encoded voltage probe
Voltage sensor domain
Fluorescence
Induced transmembrane voltage
Optical recording

ABSTRACT

The development of a high performance protein probe for the measurement of membrane potential will allow elucidation of spatiotemporal regulation of electrical signals within a network of excitable cells. Engineering such a probe requires a functional screen of many candidates. Although the glass-microelectrode technique generally provides an accurate measure of a given test probe, throughputs are limited. In this study, we focused on an approach that uses the membrane potential changes induced by an external electric field in a geometrically simple mammalian cell. For quantitative evaluation of membrane voltage probes that rely on the structural transition of the S1–S4 voltage sensor domain and hence have non-linear voltage dependencies, it was crucial to introduce exogenous inwardly rectifying potassium conductance to reduce cell-to-cell variability in resting membrane potentials. Importantly, the addition of the exogenous conductance drastically altered the profile of the field-induced potential. Following a site-directed random mutagenesis and the rapid screen, we identified a mutant of a voltage probe Mermaid, exhibiting positively shifted voltage sensitivity. Due to its simplicity, the current approach will be applicable under a microfluidic configuration to carry out an efficient screen. Additionally, we demonstrate another interesting aspect of the field-induced optical signals, ability to visualize electrical couplings between cells.

1. Introduction

Elucidating spatiotemporal flows of electrical signals within a network of excitable cells is arguably one of the most significant challenges in modern physiology. While the conventional glass-microelectrode technique permits sensitive and reliable measurements of electrical activities in a single cell or a few cells, it is difficult to address these activities spatiotemporally. Spatially resolved measurements with excellent time resolutions have been achieved with voltage-sensitive organic dyes [1–3]. However, when applied to a complex network of heterogeneous cells, it is normally difficult to discriminate the activities in specific type of cells. The use of a protein-based optical probe, which can be genetically encoded under the control of cell-type specific promoters, may enable such discrimination in measurements. Since the first report of a genetically-encoded voltage probe [4], a number of protein-based voltage probes have been engineered [5–19]. Especially, the probes based on a voltage-sensing phosphatase (e.g. VSFP2.1 [5], Mermaid [6], ElectricPk [14], ArcLight [16], VSFP-Butterfly [17]) or a microbial rhodopsin (e.g. Arch [12]) exhibit improved capabilities in reporting electrical activities than the earlier channel based probes. Thus far, individual action potentials of single neurons in vitro, voltage dynamics of a beating heart in zebrafish, spontaneous as well as sensory-evoked cortical activities in living mice, and activities at neurite branches in fly brain have been successfully detected [5–19]. In spite of the recent progresses, however, the existing protein-based voltage probes do not yet reveal the sufficiently precise spatiotemporal regulation of electrical activities in a complex excitable system. Evidently, development of a better performing probe is still essential.

In engineering a protein-based voltage probe, totally rational design has been impractical. Even a small modification, which appears minor, could lead to unexpected improvements. A representative example is found in the recent report of an engineered voltage probe, ArcLight [16]. In their report, a point mutation on the surface of a fluorescence reporter coupled to a voltage-sensor domain remarkably enhanced the responsiveness by an unknown mechanism. Thus, functional screening of many candidates is crucial for the development of a better performing probe. While simultaneous single cell photometry and voltage-clamp recordings provide accurate measurements, throughputs in hand-

* Corresponding author at: Laboratory of Integrative Physiology, Graduate School of Medicine, Osaka University, Suita, Osaka 565-0871, Japan. Tel.: +81 6 6879 3311; fax: +81 6 6879 3319.
E-mail address: tsutsui@phys2.med.osaka-u.ac.jp (H. Tsutsui).

http://dx.doi.org/10.1016/j.bbamem.2014.03.002
0005-2736/

operated patch-clamp recordings are limited. Automated electrophysiology might increase efficiency. However, the technique is still not very feasible because of its high cost and lack of flexibility in freely customizing to experimental configurations.

One approach could be a use of the membrane potential changes induced by an external electric field ($\Delta\Psi$). $\Delta\Psi$ has been also termed as "induced transmembrane voltage". Theoretical and experimental studies have quantitatively addressed the spatial distributions and temporal development of $\Delta\Psi$. The key result from these studies is that $\Delta\Psi$ can be calculated for simple cell geometries under some assumptions, and the solution is basically consistent with the experimental observations [20–29]. $\Delta\Psi$ has been actually used to observe response from a rhodopsin-based voltage probe [11].

However, as we show in this report, this approach is not directly applicable to evaluations of voltage probes that rely on the structural transition of the S1–S4 voltage sensor domain, for example, from a voltage sensing phosphatase [30], because such probes generally exhibit non-linear responses to transmembrane voltage which is the sum of $\Delta\Psi$ and the resting membrane potential. The uncertainty in resting potentials brought unavoidable ambiguity to the probe responses. In contrast, organic dyes and rhodopsin-based probes normally exhibit linear optical responses to physiologically relevant voltage changes, which do not bring such uncertainties. In this report, to overcome this issue, we stabilized resting membrane potential levels by stably introducing exogenous potassium conductance. We then show that $\Delta\Psi$ is drastically altered by the added conductance. The knowledge on $\Delta\Psi$ allowed us to evaluate the performance of a non-linear voltage probe under a conventional epi-fluorescence microscope without using the currently prevalent microelectrode techniques. Finally, we also reveal another interesting aspect of the field induced optical responses, which enable visualization of electrical couplings between cells.

2. Materials and methods

2.1. Cell preparations

N2a cells (a mouse neuroblastoma cell line) and HEK293 cells were maintained in Dulbecco's Modified Eagle Medium supplemented with 10% fetal bovine serum in a standard incubator (5% CO_2, 37 °C). Transfection was performed using Lipofectamine 2000 reagent (Invitrogen, Carlsbad, CA) according to the manufacturer's protocol. Recordings were made ~24 h post-transfection. Single N2a cells were prepared as follows. Three to five hours before recording, the medium was replaced by phosphate-buffered saline with 1 mM EDTA and nominally without calcium ion, and cells were collected by gentle mechanical dissociation. N2a cells were re-suspended in the culture medium and re-plated on a 35-mm glass-bottomed dish to isolate single cells. HEK293 cells were used for visualization of electrical couplings. Di-4-ANEPPS was loaded immediately before measurement by incubating non-transfected cells with 1 mL of loading solution that contained 5 μM Di-4-ANEPPS in Hank's Balanced Salt Solution (HBSS) for 7 to 10 min at room temperature. Cells were then washed 3 times with 1.8 mL of HBSS containing 15 mM HEPES (pH 7.4).

2.2. Optical imaging

Recordings were made using an inverted microscope (IX71; Olympus, Tokyo, Japan) equipped with a 40× objective (N.A. 1.3), a stable 75-W xenon lamp (UXL-S75XB; USHIO, Tokyo, Japan), and a C-MOS camera (Orca-Flash2.8; Hamamatsu Photonics, Hamamatsu, Japan). The camera was operated using HC-image software (Hamamatsu Photonics, Hamamatsu, Japan). In the experiment shown in Fig. 1S, another C-MOS camera (Neo, Andor Technology, Belfast, UK) which was kindly lent by a local distributor was used. A hand-made electrode unit consisting of a pair of parallel platinum wires ($\phi = 0.3$ mm) with a 7.0-mm gap was immersed into the glass-bottomed dish containing single cells. A square voltage pulse was applied by using a high-speed bipolar amplifier (BA4825; NF Corporation, Yokohama, Japan). To evaluate steady-state optical responses of protein sensors which can have slow activation kinetics at low voltage, we used a pulse of relatively long duration (600 ms), unless otherwise noted. The field strength was set at 5–6 V/mm. When higher strength was used, we sometimes recognized detrimental effects to the cells. The acquisition of images during the pulse was initiated at 400 ms after its onset. The camera exposure time was 40 ms/frame. To acquire fluorescence enough to quantify the spatial distributions of the optical responses, four consecutive images of the cells were acquired before and during the pulse, which were then time-averaged. After subtraction of dark signals, a region confined by 2 concentric circles was manually fit to the image of the membrane, which was then divided into 24 regions of interest (ROIs). Signals were integrated over the ROIs to measure fluorescence intensity (F) as a function of polar angle. A change in the fluorescence intensity by the pulse (ΔF) was normalized to the initial intensity (F) to calculate the fractional fluorescence change ($\Delta F/F$ [%]). In the experiment described in Fig. 1S, pulse duration and camera exposure time were 100 ms and 5 ms/frame, respectively. The image analyses were carried out using a homebuilt program that operates in IDL (Research Systems). The excitation filter, dichroic mirror, and emission filters used were ex535/50, dm565, and em610/75 for Di-4-ANEPPS; ex450/20, dm465, and em507/65 for mUKG; ex450/20, dm465, and em595/64 for mKOκ; and ex438/24, dm458, em483/32 for CFP, respectively.

2.3. Electrophysiology and molecular biology

Whole-cell patch clamp recordings were performed using an Axopatch 200B patch clamp amplifier (Axon Instruments). The pipette solution contained (in mM): NaCl 5, KCl 10, HEPES 10, KOH 130, MgATP 2.5, Na_2GTP 0.3, and EGTA 1 (pH adjusted to 7.3 with methanesulfonic acid). The bath solution was HBSS containing 15 mM HEPES (pH 7.4). The pipette resistance ranged between 4 and 6 MΩ. Simultaneous photometry was performed as described previously [6]. Plasmids were constructed using conventional molecular biology techniques. Site-directed random mutagenesis was performed as described previously [31].

2.4. Generation of a stable N2a-kir cell line

DNA encoding the mouse Kir2.1 channel was subcloned into pEF6 vector (Invitrogen). After transfecting N2a cells with the plasmid, stable transformants were screened by culturing cells in the presence of Blasticidin (10 μg/mL) for 2 weeks. Several single colonies of cells were then passaged, from which a clonal line showing normal growth was selected and used in subsequent measurements (N2a-kir cells).

3. Results

3.1. Characterization of $\Delta\Psi$ in a normal N2a cell

We used undifferentiated N2a cells as a cell platform because almost spherical cells can be easily prepared as shown below. While $\Delta\Psi$ has been experimentally characterized in various types of cells, $\Delta\Psi$ in an N2a cell has not been reported (to our knowledge). Also, strictly, actual $\Delta\Psi$ is dependent on the specific experimental conditions. We therefore started with a system calibration experiment of $\Delta\Psi$ in an N2a cell under our experimental setup using an organic voltage-sensitive dye, Di-4-ANEPPS [32]. Similar calibration experiments in a CHO cell have been visually described previously [33].

It is generally known that $\Delta\Psi$ reaches steady-state rapidly (~ microseconds), and is linearly related to the field strength unless exceeding the limit that stimulates electroporation or membrane breakdown [22–29]. We first confirmed such basic properties in a single N2a cells (Fig. S1). To establish a quantitative measurement, we then focused

on spherical cells. In a spherical cell, when the membrane conductivity is sufficiently low compared to the aqueous phase, $\Delta\Psi$ in the middle of the cell in a steady state can be analytically described as:

$$\Delta\Psi = 1.5\,ER\,Cos\theta \quad (1)$$

where, E, R, and θ are the external electric field, radius of the cell, and the polar angle from the center of the cell with respect to the field direction, respectively [20,21] (Fig. 1A). Eq. (1) has been often referred to as Schwan's equation. An isolated cell with a nearly spherical shape that was still sufficiently attached to the glass substrate could be easily prepared by re-plating cells which have been gently dissociated from confluent culture onto a glass-substrate (Fig. 1B). Such a cell was again loaded with Di-4-ANEPPS and subjected to a pulse of electric field. Resulting spatial distributions of the fractional changes in fluorescence ($\Delta F/F$) were analyzed. Both the depolarizing (loss of fluorescence) and hyperpolarizing (gain of fluorescence) responses were observed at both the cathodic and the anodic sides of the membrane (Fig. 1C). We analyzed the angle dependency of $\Delta F/F$ and confirmed a linear correlation between $\Delta F/F$ and Cosθ (Fig. 1D, E), reflecting the validity of Eq. (1) in our experimental setting. We calibrated optical signals from Di-4-ANEPPS by means of voltage-clamp recordings in order to relate $\Delta F/F$ to the actual membrane potential change (Fig. 1F). Fig. 1G shows a plot of the calibrated $\Delta\Psi$ as a function of ERCosθ. The coefficient (i.e., slope) determined from our experiments was ~1.07 and was lower than the value of 1.5 expected from Eq. (1). Lower values of coefficients have been similarly reported in other types of cells [24,26,27], which most likely reflect realistic aspects of actual biological cells including non-zero membrane conductivity.

3.2. Variations in the optical responses from a non-linear, protein-based voltage probe

As described above, we observed that the spatial distribution of $\Delta\Psi$ under our experimental conditions approximately follows a modified form of Eq. (1):

$$\Delta\Psi = \alpha ER\,Cos\theta \quad (2)$$

$$\alpha \approx 1.07 \quad (3)$$

where α is the experimentally determined coefficient (Fig. 1G). We performed a pilot evaluation of a voltage probe, Mermaid [6], using this equation. Upon depolarization, Mermaid exhibits a gain of Förster resonance energy transfer (FRET) between a pair of fluorescent proteins:

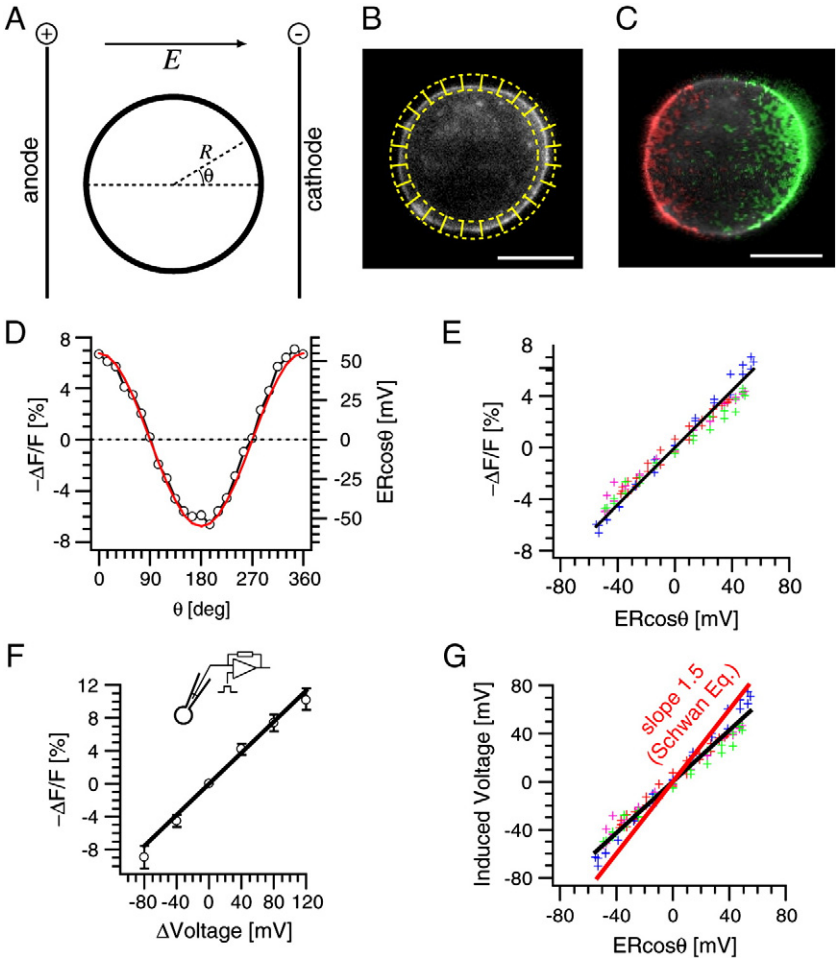

Fig. 1. Field-induced membrane potential in a spherical N2a cell. A. A scheme showing the electrodes, cell, and parameters (E, R, θ) used in the present study. The illustration is not to scale. The gap between the electrodes is 7 mm. B. A roughly spherical cell was analyzed. The grids in yellow shows 24 regions of interest used to analyze the angle dependency of the optical responses. C. A pseudo-colored optical response in an N2a cell loaded with Di-4-ANEPPS, with a field strength of 5 V/mm and a threshold set at 4%. Regions exhibiting negative (depolarizing; $\Delta F/F < -4\%$) and positive (hyperpolarizing; $\Delta F/F > 4\%$) responses were highlighted in green and red, respectively. D. A representative plot of $-\Delta F/F$ as a function of θ (open circles). The red line indicates a curve for ERCosθ [mV]. E. A plot showing $-\Delta F/F$ versus ERCosθ in 4 different cells. Data from each cell were plotted in the same color (cross shapes). The solid line indicates a linear fit ($-\Delta F/F$ [%] = 0.111 ERCosθ [mV]). F. Calibration of $\Delta F/F$ with voltage-clamp recordings. Data show the mean ± standard deviations (S.D.) in 5 different cells (open circles). The solid line indicates a linear fit ($-\Delta F/F$ [%] = 0.105 ΔVoltage [mV]). The holding potential was −60 mV. G. A plot of induced voltage versus ERCosθ. Data in E are plotted using the calibration data in F. The black and red lines indicate a linear fit ($\Delta\Psi$ [mV] = 1.067 ERCosθ [mV]) and Schwan's equation (slope = 1.5), respectively. Bars = 10 μm (B, C).

mUKG and mKOκ (Fig. 2A). Spherical cells expressing Mermaid were subjected to an electric field as in the section before. As expected from the nature of FRET, the donor and acceptor signals are reciprocal

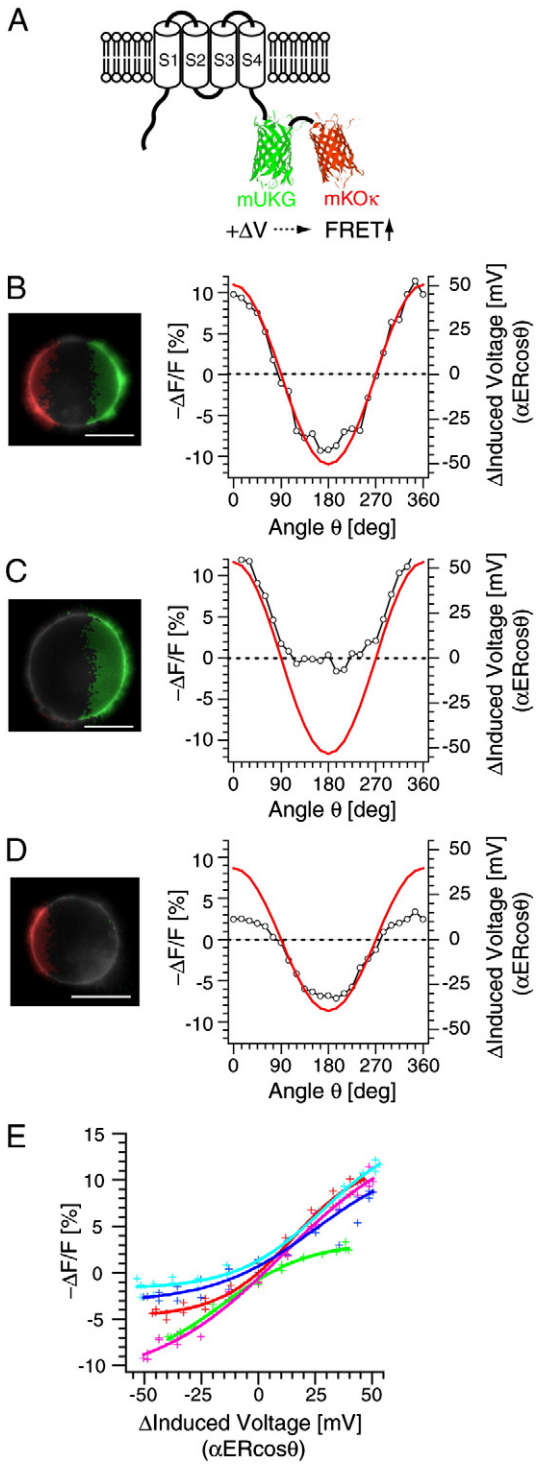

Fig. 2. Field-induced optical response of Mermaid in N2a cells. A. Schematic illustration of a voltage probe, Mermaid, consisting of a S1–S4 voltage sensor domain and a FRET reporter [6]. B–D. Three representative field-induced optical responses of Mermaid in normal N2a cells. Pseudo-colored images of the responses are shown on the left. The field strength is 5 V/mm. Regions showing a decrease or increase in fluorescence are highlighted in green and red, respectively (threshold = ±4%). The plots on the right show −ΔF/F as a function of θ (open circles). The red lines indicate the induced membrane potential change estimated using Eqs. (2) and (3). Bars = 10 μm. E. Optical responses (−ΔF/F) as a function of estimated induced membrane potential change (i.e., αERCosθ; α = 1.07) in 5 different cells. Data are indicated by cross shapes. Solid lines indicate Boltzmann fits. Vmid was 12.5 ± 16.9 mV (average ± S.D.).

(Fig. S2). The donor (i.e. mUKG) signals were then subject to quantitative analysis. We found large significant variations in the profiles of the optical responses depending on the individual cell. In some cells, both the depolarizing (negative ΔF/F) and the hyperpolarizing (positive ΔF/F) responses were observed on both sides of the membrane, as with Di-4-ANEPPS (Fig. 2B), but other cells showed noticeable responses only on one side of the membrane (Fig. 2C, D). Fig. 2E shows a plot of the observed ΔF/F versus ΔΨ calculated using Eqs. (2) and (3) in 5 different cells, showing large variations in responses. Considering that Mermaid exhibits non-linear, sigmoidal responses to actual membrane potential which is the sum of ΔΨ and resting membrane potential (E_{rest}), we reasoned that the observed diversity in the optical response reflects the variation in E_{rest}. This is not the case with Di-4-ANEPPS, because the dye exhibits a linear response over a wide range of membrane voltage values; hence, ΔF/F does not depend on E_{rest}. We measured resting potentials in our preparations of N2a cells using the whole-cell patch-clamp recordings and in fact confirmed significant variations in E_{rest} (−25.4 ± 10.2 mV, n = 16 cells). Although a qualitative evaluation of a given probe may be possible using a plot such as the one shown in Fig. 2E, we sought to establish a more quantitative evaluation.

3.3. ΔΨ in an N2a cell stably expressing Kir2.1 channel

In an attempt to reduce variations in E_{rest}, we generated a stable line of N2a cells expressing the inwardly-rectifying potassium channel Kir2.1, which plays a role in the maintenance of hyperpolarized resting membrane potentials in various types of cells [34,35]. The established cell line (N2a-kir cells) revealed hyperpolarized E_{rest} that was significantly reduced in variation (−88.8 ± 3.3 mV, n = 10 cells; Fig. S3). To investigate the profile of ΔΨ induced in an N2a-kir cell, we characterized ΔΨ using Di-4-ANEPPS. Remarkably, in contrast to normal cells (i.e., cells not expressing Kir2.1) that exhibited both depolarizing and hyperpolarizing responses at the membrane on both sides of the electrode (Fig. 1C), N2a-kir cells exhibited a totally distinct ΔΨ profile: depolarizing responses were observed at all angles except for the most anodic end (Fig. 3A). The observation is reasonable if we consider a simplified situation as follows. Assumed that Kir2.1 channel provides a diode-like asymmetrical conductance exhibiting negligible resistance to the current influx but a high resistance to the efflux, the hyperpolarizing response that occurred most extensively at the anodic end in normal cells (i.e., without Kir2.1 channels) is balanced out via local influx in N2a-kir cells. As a result, depolarizing responses develop in the other regions where there is no significant counteracting efflux upon depolarization because of the asymmetrical nature of Kir2.1 conductance. The intracellular potential will still be uniform, as in normal cells without Kir2.1, because the net current passing through a cell is negligible in the steady state. This also ensures that the potential outside a Kir2.1 cell is not significantly distorted from that around a normal cell. Alternatively, an N2a-kir cell under an external electric field can be simplified as being analogous to a cell in which the membrane at the anodic end is locally porated. Notably, Hibino et al. [25] have theoretically investigated ΔΨ in such a situation, which revealed a ΔΨ profile that is very similar to the observation. Considering their study [25], when membrane conductivity and thickness are again sufficiently low except for the anodic end, ΔΨ in such a situation is approximated by 1.5 ER(Cosθ + 1).

We analyzed experimental data of Di-4-ANEPPS signals as a function of the angle θ, and found relatively good proportionality of ΔΨ to ER(Cosθ + 1) (Fig. 3B, C). We employed a linear fit. The coefficient (i.e., slope) determined from the data is ~1.02. From these results, we empirically found that ΔΨ in our N2a-kir cell is approximately given by:

$$\Delta\Psi = \beta ER(\mathrm{Cos}\theta + 1) \tag{4}$$

$$\beta \approx 1.02 \tag{5}$$

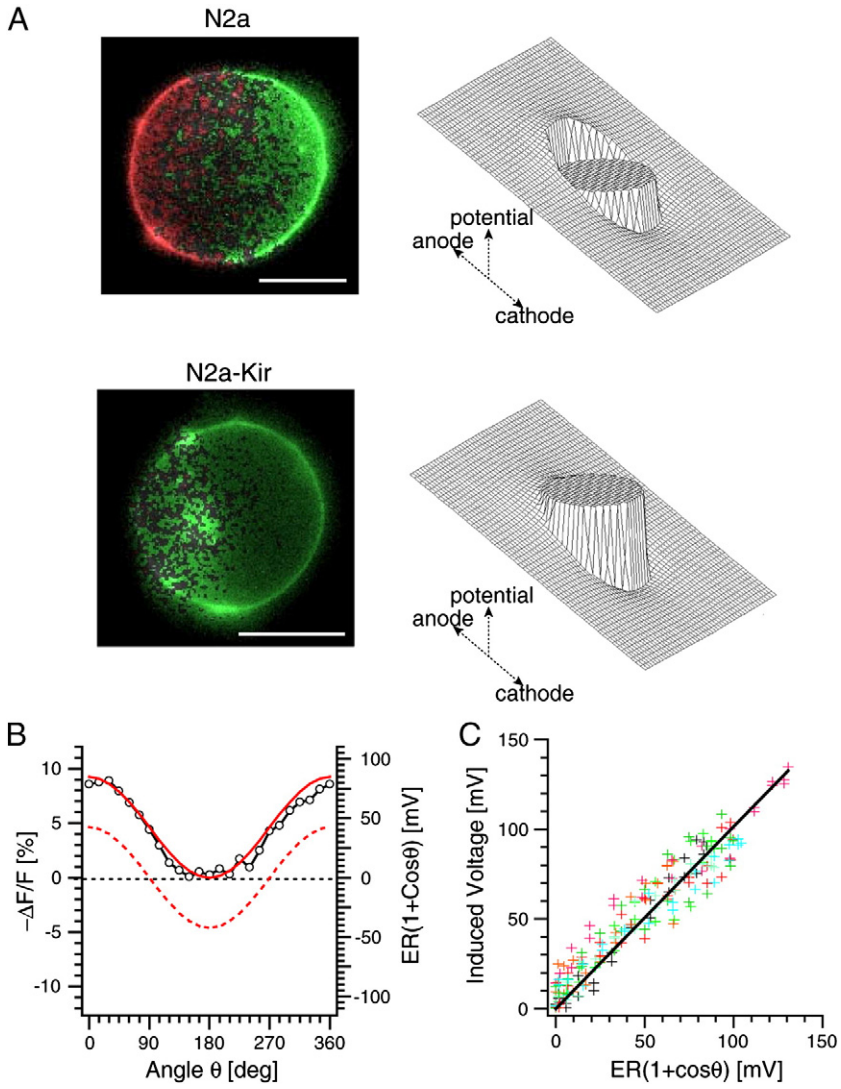

Fig. 3. Field-induced membrane potential in an N2a-kir cell probed with Di-4-ANEPPS. A. Pseudo-colored optical response in an N2a-kir cell loaded with Di-4-ANEPPS (bottom left). The response of a normal N2a cell is shown as a reference (the data used is the same as in Fig. 1C; top left). The threshold is set at ±2%, and the field strength is 5 V/mm. Regions exhibiting negative (depolarizing) and positive (hyperpolarizing) responses are highlighted in green and red, respectively. Bars = 10 μm. The predicted profile of the potential around a cell with a non-conductive membrane (top right) and that around a cell in which the membrane at the anodic end is locally porated (bottom right) are graphically shown. These profiles were generated in accordance with a previous theoretical study (Hibino et al. [25]). B. A representative plot of optical responses (−ΔF/F) in an N2a-kir cell as a function of θ (open circles). The solid and dashed red lines indicate the curves for ER(1 + Cosθ) and ERCosθ, respectively. C. Induced membrane potential changes as a function of ER(1 + Cosθ) for 9 different cells. The solid line indicates a linear fit (slope = 1.02).

where β is a compensation factor for N2a-kir cells under our experimental conditions.

3.4. Evaluation using an N2a-kir cell

As just described, an N2a-kir cell provides a platform in which E_{rest} and $\Delta\Psi$ are both defined. Then we retried the measurement of Mermaid. In an N2a-kir cell, Mermaid as well exhibited entirely depolarizing responses except for the region at the anodic end (Fig. 4A). Fig. 4B shows a representative plot of optical responses (ΔF/F) as a function of θ. Because of the nonlinear voltage-dependency of Mermaid, the angle dependency of ΔF/F deviated from the curve of Cosθ + 1 (Fig. 4B). Fig. 4C shows the plots of Mermaid responses versus $E_{rest} + \Delta\Psi$ for 6 different cells, where E_{rest} was set at an average value (−89 mV) and Eqs. (4) and (5) were used to determine $\Delta\Psi$. As observed, responses from Mermaid were more consistent in N2a-kir cells than in normal cells (Figs. 2C, 4C). The response of each cell was fit with a Boltzmann function. The averaged V_{mid} was −46.3 mV ± 4.9 mV (average ± S.D.; n = 6 cells), which was in good agreement with the values obtained electrophysiologically (−42.8 ± 4.1 mV; n = 6) (Fig. 4C). The evaluation also gave maximum fluorescence decreases ($-\Delta F/F_{max}$; 14.6 ± 1.4%; n = 6) comparable to those obtained with electrophysiological recordings (16.3 ± 2.3%; n = 6). Moreover, we performed evaluation of another voltage probe Mermaid2 [18] (Fig. S4), which likewise confirmed that a non-linear, protein-based probe can be quantitatively evaluated by analyzing the response to a single electric field pulse in an N2a-kir cell.

3.5. A rapid screen of Mermaid-D129X mutants

Finally, aiming to examine the validity of the present approach as a way to screen protein probes, we evaluated several mutant probes generated by site-directed random substitutions. We focused on residue D129 of Mermaid, which is located in S1 and is homologous to Kv1.2 Glu183, the putative salt bridge partner of R3 in the open state of the protein [36] (Fig. 5A). Although we previously found that the D129R mutation eliminates responses to voltage change in a physiologically relevant range [9], the effects of other mutations have not been addressed. Following the site-directed random mutagenesis of D129, we

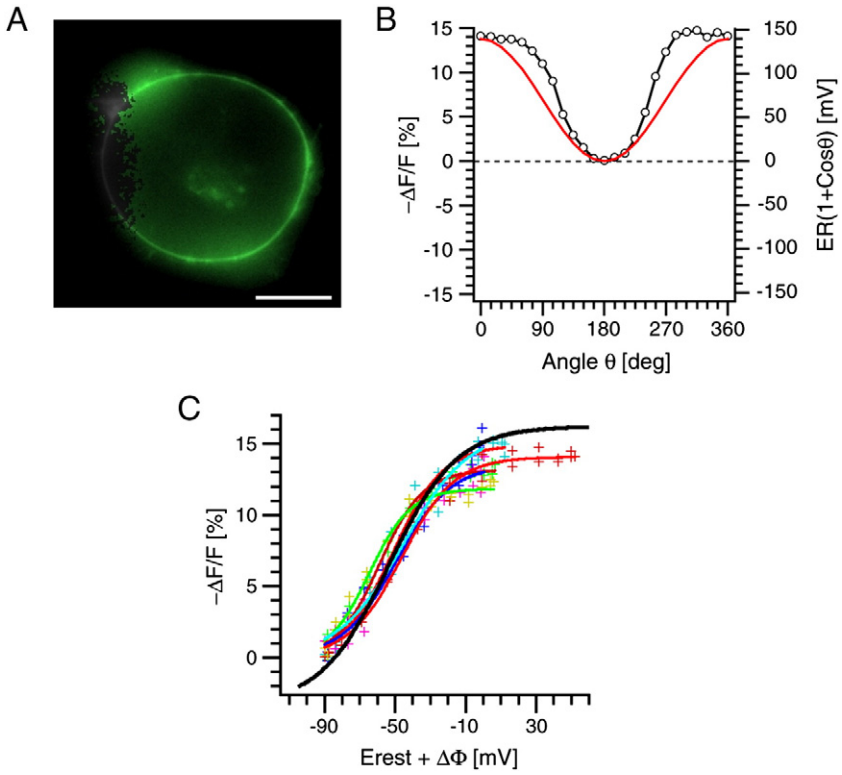

Fig. 4. Evaluation of Mermaid using N2a-kir cells. A. Pseudo-colored optical response in an N2a-kir cell expressing Mermaid. The threshold is set to ±2%, and the field strength at 6 V/mm. Bar = 10 μm. B. A representative plot of −ΔF/F as a function of θ (open circles). The red line indicates a curve for ER(1 + Cosθ). C. Plots of −ΔF/F versus E_{rest} + ΔΨ for 6 different cells. E_{rest} was set at −88 mV. ΔΨ was predicted using Eqs. (4) and (5). Colored solid lines indicate Boltzmann fits. An averaged response obtained with patch-clamp recordings for six cells is superimposed (thick black line).

obtained 6 different mutants: Mermaid_D129H, L, E, R, Q, and W. These mutants were then evaluated using our current approach. We first evaluated D129R and found null optical responses for all angles (Fig. 5), which confirmed the previous electrophysiological result [9]. D129H, L, Q, and W mutants similarly exhibited null responses (Fig. S5), thus demonstrating the functional significance of the residue. Of the 6 mutants, only D129E showed clear optical responses. In contrast to Mermaid (Fig. 4A), D129E exhibited optical responses only at the cathodic side of the membrane (Fig. 5E, F). Such a profile indicates a positive shift in the voltage dependence of the probe, as is clearly shown in the plot of ΔF as a function of E_{rest} + ΔΨ. The V_{mid} value in Mermaid-D129E was 19 mV ± 11 mV (average ± S.D., n = 6 cells), which agreed well with data obtained with patch-clamp recording (V_{mid} = ~22.5 mV; Fig. 5G). In this way, the current approach enables rapid characterizations of mutant probes using a single electric field pulse.

4. Discussion

While the basal potassium permeability largely contributes to the resting membrane potential, it is difficult to rapidly control membrane potential over a physiologically relevant voltage range only by changing the external potassium concentration. Simultaneous photometry and patch-clamp recording is currently the prevalent method that provides an accurate measure of a given probe. But, the throughputs are limited. Aiming to fill the gap, we developed a simple approach using the spatial distribution of field-induced membrane potential change (ΔΨ). We showed that the performance of a given probe can be quantitatively evaluated with a single pulse of electric field. Although the evaluations may be less accurate than those by genuine voltage-clamp recordings, the procedure does not require skillful manipulations of microelectrodes and thus potentially has higher throughputs. As a proof of principle experiment, we evaluated 6 different mutants of Mermaid and found that Mermaid-D129E has a positively shifted voltage sensitivity (V_{mid} = ~20 mV). Such a probe may be used for analyses of electrical activities that occur dynamically in a positive voltage range, for example, the voltage dynamics in activated neutrophils [37]. Image analysis is the major part of the current approach. While we performed it almost manually in this study, we believe that most of the steps including cell identifications can be done automatically. Considering this point as well as the simplicity of the procedures, the current approach can be potentially incorporated into a microfluidic device to build an efficient screening system [38]. In addition, considering that ΔΨ is thought to reach a steady state in the order of microseconds [21,28], not only the steady state response but also the kinetic aspects of test probes may be evaluated using a fast camera. This, however, will require substantial averaging of many trials. Such efforts are in progress.

We introduced Kir2.1 channel to reduce variations in E_{rest} of N2a cells. This had a remarkable effect on ΔΨ (Fig. 3). Generally, profiles of ion channels determine many important cellular properties such as the cytoplasmic ionic environments, resting membrane potentials and membrane excitabilities. The present result clearly demonstrated that electrical response to an external electric field is also a function of ion channel profile. Given that the endogenous electric field appears to have a variety of physiological functions [39,40], it is conceivable that ion channels may play an important role in tuning physiological responses to such endogenous fields.

Finally, in the course of the present study, we noticed another interesting point: the ability to reveal a pattern of electrical couplings between cells by the field-induced optical responses. Using an organic voltage-sensitive dye is more straightforward for this purpose because of the linearity of its response. An isolated cell normally exhibits both depolarizing and hyperpolarizing responses upon application of an

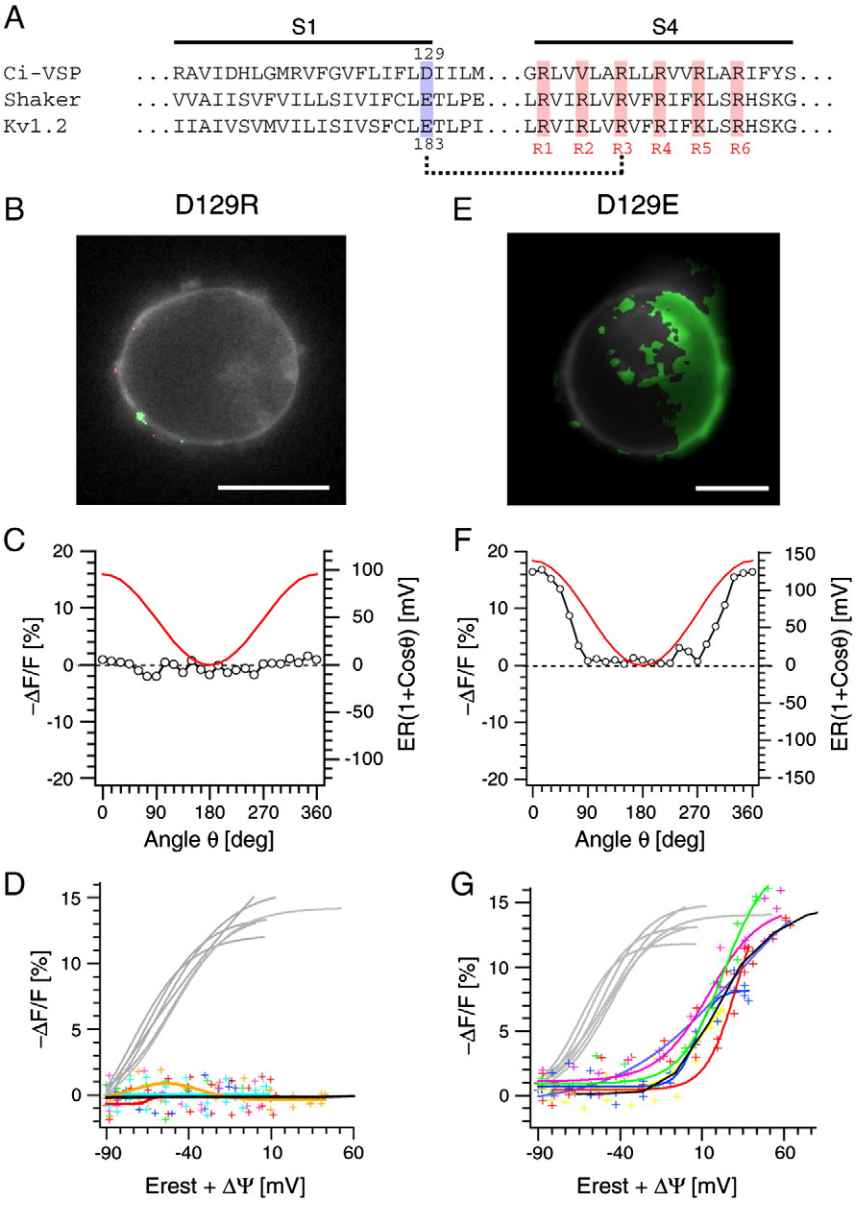

Fig. 5. Effect of D129R and D129E mutations in Mermaid. A. Amino-acid sequence (single-letter code) alignment of Ci-VSP, Shaker, and Kv1.2 for S1 and S4. The dotted line indicates the salt bridge interaction between E183 and the third Arginine residue in the S4 segment (R3) as predicted in the crystal structure by Long et al. [36]. B. E. Images show optical response in D129R (B) and D129E (E) mutants. The threshold is ±2%, and the field strength is 6 V/mm. Bars = 10 μm. C, F. A representative plot of optical response (−ΔF/F) in D129R (C) and D129E (F) as a function of θ (open circles). The solid lines indicate the curves for ER(1 + Cosθ). D, G. Optical response (−ΔF/F) as a function of $E_{rest} + \Delta\Psi$ in D129R (D; n = 9 cells) and D129E (G; n = 6 cells) mutants. The solid line indicates Boltzmann fits. The responses measured with patch-clamp recordings were superimposed in black lines. The gray lines indicate responses in Mermaid as a reference (data from Fig. 4C).

external electric field at the membrane on both the cathodic and anodic sides, as shown (Fig. 1C). In contrast, we sometimes observed that whole cells exhibited the depolarizing response while an adjacent cell on the side of the cathode showed an entirely hyperpolarizing response, suggesting that the two cells were electrically coupled and behaved like a single cell. We show a typical example in HEK293 cells (Fig. 6A).

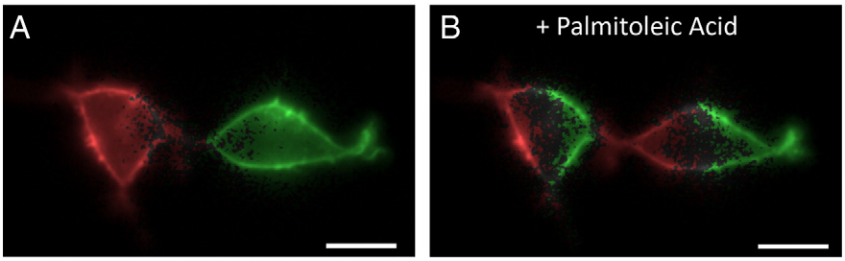

Fig. 6. Visualization of an electrical coupling. A, B. Normal HEK293 cells loaded with Di-4-ANEPPS and subjected to a pulse of electric field strength of 4.3 V/mm. The image shows the pseudo-colored optical responses of 2 neighboring cells before (A) and after (B) treatment with the gap junction uncoupler, palmitoleic acid (100 μM). The threshold is 2%. Regions exhibiting negative (depolarizing) and positive (hyperpolarizing) responses are highlighted in green and red, respectively. Bars = 10 μm.

Treatment with palmitoleic acid, a gap junction uncoupler [41], altered the optical response of individual cells to one that is typically seen in an isolated single cell (Fig. 6B). In this way, we demonstrated that a pattern of electrical coupling can be functionally visualized using optical responses under application of an electric field pulse.

Acknowledgements

We are grateful to Dr. K. Kinosita for helpful discussion and Dr. Y. Kubo for providing cDNA encoding Kir2.1 channel. We also thank the members of laboratory of integrative physiology for comments and discussions. This work was supported by grants from JST-PRESTO program (H.T.) and MEXT (#23115712).

Appendix A. Supplementary data

Supplementary data to this article can be found online at http://dx.doi.org/10.1016/j.bbamem.2014.03.002.

References

[1] A. Grinvald, B.M. Salzberg, L.B. Cohen, Simultaneous recording from several neurones in an invertebrate central nervous system, Nature 268 (1977) 140–142.
[2] B.M. Salzberg, A. Grinvald, L.B. Cohen, H.V. Davila, W.N. Ross, Optical recording of neuronal activity in an invertebrate central nervous system: simultaneous monitoring of several neurons, J. Neurophysiol. 40 (1977) 1281–1291.
[3] D. Gross, L.M. Loew, Fluorescent indicators of membrane potential: microspectrofluorometry and imaging, Methods Cell Biol. 30 (1989) 193–218.
[4] M.S. Siegel, E.Y. Isacoff, A genetically encoded optical probe of membrane voltage, Neuron 19 (1997) 735–741.
[5] D. Dimitrov, Y. He, H. Mutoh, B.J. Baker, L. Cohen, W. Akemann, T. Knopfel, Engineering and characterization of an enhanced fluorescent protein voltage sensor, PLoS One 2 (2007) e440.
[6] H. Tsutsui, S. Karasawa, Y. Okamura, A. Miyawaki, Improving membrane voltage measurements using FRET with new fluorescent proteins, Nat. Methods 5 (2008) 683–685.
[7] A. Perron, H. Mutoh, T. Launey, T. Knopfel, Red-shifted voltage-sensitive fluorescent proteins, Chem. Biol. 16 (2009) 1268–1277.
[8] W. Akemann, H. Mutoh, A. Perron, J. Rossier, T. Knopfel, Imaging brain electric signals with genetically targeted voltage-sensitive fluorescent proteins, Nat. Methods 7 (2010) 643–649.
[9] H. Tsutsui, S. Higashijima, A. Miyawaki, Y. Okamura, Visualizing voltage dynamics in zebrafish heart, J. Physiol. 588 (2010) 2017–2021.
[10] B.J. Baker, L. Jin, Z. Han, L.B. Cohen, M. Popovic, J. Platisa, V. Pieribone, Genetically encoded fluorescent voltage sensors using the voltage-sensing domain of *Nematostella* and *Danio* phosphatases exhibit fast kinetics, J. Neurosci. Methods 208 (2012) 190–196.
[11] J.M. Kralj, D.R. Hochbaum, A.D. Douglass, A.E. Cohen, Electrical spiking in *Escherichia coli* probed with a fluorescent voltage-indicating protein, Science 333 (2011) 345–348.
[12] J.M. Kralj, A.D. Douglass, D.R. Hochbaum, D. Maclaurin, A.E. Cohen, Optical recording of action potentials in mammalian neurons using a microbial rhodopsin, Nat. Methods 9 (2012) 90–95.
[13] A.J. Lam, F. St-Pierre, Y. Gong, J.D. Marshall, P.J. Cranfill, M.A. Baird, M.R. McKeown, J. Wiedenmann, M.W. Davidson, M.J. Schnitzer, R.Y. Tsien, M.Z. Lin, Improving FRET dynamic range with bright green and red fluorescent proteins, Nat. Methods 9 (2012) 1005–1012.
[14] L. Barnett, J. Platisa, M. Popovic, V.A. Pieribone, T. Hughes, A fluorescent, genetically-encoded voltage probe capable of resolving action potentials, PLoS One 7 (2012) e43454.
[15] L. Jin, B. Baker, R. Mealer, L. Cohen, V. Pieribone, A. Pralle, T. Hughes, Random insertion of split-cans of the fluorescent protein venus into Shaker channels yields voltage sensitive probes with improved membrane localization in mammalian cells, J. Neurosci. Methods 199 (2011) 1–9.
[16] L. Jin, Z. Han, J. Platisa, J.R. Wooltorton, L.B. Cohen, V.A. Pieribone, Single action potentials and subthreshold electrical events imaged in neurons with a fluorescent protein voltage probe, Neuron 75 (2012) 779–785.
[17] W. Akemann, H. Mutoh, A. Perron, Y.K. Park, Y. Iwamoto, T. Knopfel, Imaging neural circuit dynamics with a voltage-sensitive fluorescent protein, J. Neurophysiol. 108 (2012) 2323–2337.
[18] H. Tsutsui, Y. Jinno, A. Tomita, Y. Niino, Y. Yamada, K. Mikoshiba, A. Miyawaki, Y. Okamura, Improved detection of electrical activity with a voltage probe based on a voltage-sensing phosphatase, J. Physiol. 591 (2013) 4427–4437.
[19] G. Cao, J. Platisa, V.A. Pieribone, D. Raccuglia, M. Kunst, M.N. Nitabach, Genetically targeted optical electrophysiology in intact neural circuits, Cell 154 (2013) 904–913.
[20] H.P. Schwan, Electrical properties of tissue and cell suspensions, Adv. Biol. Med. Phys. 5 (1957) 147–209.
[21] K.S. Cole, Membranes, Ions and Impulses, University of California Press, Berkeley, CA, 1972.
[22] D. Gross, L.M. Loew, W.W. Webb, Optical imaging of cell membrane potential changes induced by applied electric fields, Biophys. J. 50 (1986) 339–348.
[23] B. Ehrenberg, D.L. Farkas, E.N. Fluhler, Z. Lojewska, L.M. Loew, Membrane potential induced by external electric field pulses can be followed with a potentiometric dye, Biophys. J. 51 (1987) 833–837.
[24] Z. Lojewska, D.L. Farkas, B. Ehrenberg, L.M. Loew, Analysis of the effect of medium and membrane conductance on the amplitude and kinetics of membrane potentials induced by externally applied electric fields, Biophys. J. 56 (1989) 121–128.
[25] M. Hibino, M. Shigemori, H. Itoh, K. Nagayama, K. Kinosita Jr., Membrane conductance of an electroporated cell analyzed by submicrosecond imaging of transmembrane potential, Biophys. J. 59 (1991) 209–220.
[26] C. Grosse, H.P. Schwan, Cellular membrane potentials induced by alternating fields, Biophys. J. 63 (1992) 1632–1642.
[27] J. Teissie, M.P. Rols, An experimental evaluation of the critical potential difference inducing cell membrane electropermeabilization, Biophys. J. 65 (1993) 409–413.
[28] G. Pucihar, T. Kotnik, B. Valic, D. Miklavcic, Numerical determination of transmembrane voltage induced on irregularly shaped cells, Ann. Biomed. Eng. 34 (2006) 642–652.
[29] T. Kotnik, D. Miklavcic, Analytical description of transmembrane voltage induced by electric fields on spheroidal cells, Biophys. J. 79 (2000) 670–679.
[30] Y. Murata, H. Iwasaki, M. Sasaki, K. Inaba, Y. Okamura, Phosphoinositide phosphatase activity coupled to an intrinsic voltage sensor, Nature 435 (2005) 1239–1243.
[31] A. Sawano, A. Miyawaki, Directed evolution of green fluorescent protein by a new versatile PCR strategy for site-directed and semi-random mutagenesis, Nucleic Acids Res. 28 (2000) E78.
[32] E. Fluhler, V.G. Burnham, L.M. Loew, Spectra, membrane binding, and potentiometric responses of new charge shift probes, Biochemistry 24 (1985) 5749–5755.
[33] G. Pucihar, T. Kotnik, D. Miklavcic, Measuring the induced membrane voltage with Di-8-ANEPPS, J. Vis. Exp. 33 (2009) 1659.
[34] Y. Kubo, T.J. Baldwin, Y.N. Jan, L.Y. Jan, Primary structure and functional expression of a mouse inward rectifier potassium channel, Nature 362 (1993) 127–133.
[35] C.G. Nichols, A.N. Lopatin, Inward rectifier potassium channels, Annu. Rev. Physiol. 59 (1997) 171–191.
[36] S.B. Long, X. Tao, E.B. Campbell, R. MacKinnon, Atomic structure of a voltage-dependent K+ channel in a lipid membrane-like environment, Nature 450 (2007) 376–382.
[37] A. Jankowski, S. Grinstein, A noninvasive fluorimetric procedure for measurement of membrane potential. Quantification of the NADPH oxidase-induced depolarization in activated neutrophils, J. Biol. Chem. 274 (1999) 26098–26104.
[38] J. Godin, C.H. Chen, S.H. Cho, W. Qiao, F. Tsai, Y.H. Lo, Microfluidics and photonics for Bio-System-on-a-Chip: a review of advancements in technology towards a microfluidic flow cytometry chip, J. Biophotonics 1 (2008) 355–376.
[39] C.D. McCaig, A.M. Rajnicek, B. Song, M. Zhao, Controlling cell behavior electrically: current views and future potential, Physiol. Rev. 85 (2005) 943–978.
[40] F. Frohlich, D.A. McCormick, Endogenous electric fields may guide neocortical network activity, Neuron 67 (2010) 129–143.
[41] J.M. Burt, K.D. Massey, B.N. Minnich, Uncoupling of cardiac cells by fatty acids: structure–activity relationships, Am. J. Physiol. 260 (1991) C439–C448.